TECHNISCHE MECHANIK
an open access journal

journal homepage: www.ovgu.de/techmech

Tech. Mech., Vol. 45, Is. 1, (2025), 24–30

Received: 13.04.2025
Accepted: 16.06.2025
Available online: 16.06.2025

Damage prediction in fiber reinforced plastic sandwich structures for marine applications under dynamic loading

Norman Osa-Uwagboe[1,2⋆], Vadim V. Silberschmidt[1], Emrah Demirci[1],

[1] Wolfson School of Mechanical, Electrical and Manufacturing Engineering, Loughborough University, LE11 3TU, UK.
[2] Air Force Research and Development Centre, Nigerian Air Force Base, Kaduna, PMB 2104, Nigeria.

Abstract: Fibre reinforced plastic sandwich structures (FRPSSs) are increasingly popular in marine applications thanks to their high stiffness, lightweight, good buoyancy, and damage resistance. These structures are often subjected to foreign-object damage in the form of low-velocity impacts. In this study, an in situ acoustic emission methodology was employed to monitor seawater ingress into FRPSS samples with varying core configurations until saturation and subsequently samples were subjected to large-deflection impact bending tests. The obtained results indicated that the moisture uptake led to a reduction in impact bending capacity. Notably, there was a negligible change in energy-absorption performance after exposure. Post-exposure assessment of the damage morphology revealed extensive core shearing, delamination, core/face sheet debonding, and fibre breakage as major failure modes.

Keywords: Composite sandwich, X-ray micro-CT, damage, seawater exposure, acoustic emission, low-velocity impact.

1 Introduction

FRP sandwich structures (FRPSSs) are composite materials typically constructed from stiffer, thin face sheets bonded to a weaker core. Thanks to the increasing demand for lightweight, efficient, and high-performance materials, resulted in significant increase in recent years in the use of FRPSSs. Their properties led to widespread application in critical components in the automotive, aerospace, defense, and maritime industries thanks to their low weight, high strength, ease of manufacturing, cost-effectiveness, good corrosion resistance, and buoyancy Osa-Uwagboe et al. (2023b); Feng and Aymerich (2013). The mechanical behaviour of FRPSS, primarily influenced by performance of its constituents, particularly the bond between the face sheet and the core, and their combined ability to resist damage. While the intrinsic properties of the materials are crucial, the operational environment can also significantly impact the performance of structures over time. For instance, FRPSSs used in marine environments are prone to degradation caused by moisture absorption, which negatively affects the matrix and interfacial bonding at various scales Robin et al. (2023); Osa-Uwagboe et al. (2024); Qiu et al. (2023). A common loading regime of FRPSSs in marine applications is foreign-object low-velocity impact, which often results in barely visible impact damage (BVID). The presence of BVID combined with seawater ageing can exacerbate the deterioration of the structure, potentially leading to catastrophic failure. Common damage modes associated with seawater exposure include accelerated matrix cracking, facesheet buckling, laminate delamination, and debonding between the facesheets and the core. To investigate the damage behaviour of FRPSSs, researchers have employed various testing methods, such as drop weight, quasi-static indentation, and IZOD impact tests Feng and Aymerich (2013); Osa-Uwagboe et al. (2023a); Chai and Zhu (2011). Studies showed that facesheet configuration significantly influenced the energy absorption capacity of FRPSS compared to core variations. Predictive damage models were also developed for foam-core FRPSSs. While substantial work was done on the in-plane characteristics of FRPSSs used in marine application, their out-of-plane behaviour, particularly the impact bending properties, are still unclear. In this study, the impact behaviour of FRPSS under single impact before and after seawater exposure are investigated with a view to understand their damage behaviour, which could be useful in material optimization.

2 Experimental methodology

2.1 Material properties

FRPSS samples were made from E-glass plain weave fabric with 160 g/m^2 from Samson Composites Ltd (Shenzhen, China) with epoxy resin from EPOCHEM Ltd (Lagos, Nigeria) at a volumetric ratio of 2:1. EASYCell 75 closed-cell PVC foam core composites (Stoke-on-Trent, UK) was used as the core. The samples were fabricated at room temperature (27 °C in Nigeria). and allowed to cure for 18 hours with 4 layers each for the top and bottom face sheets. The fabrication process used was the hand lay-up and a vacuum-bagging technique and sample plates of 80 mm × 80 mm with 3 different core configurations as shown in Fig. 1. Details of the mechanical properties of the samples analysed and their configurations are presented in Tab. 1 and Tab. 2.

⋆ E-mail address: n.osa-uwagboe@lboro.ac.uk
doi: 10.24352/UB.OVGU-2025-038

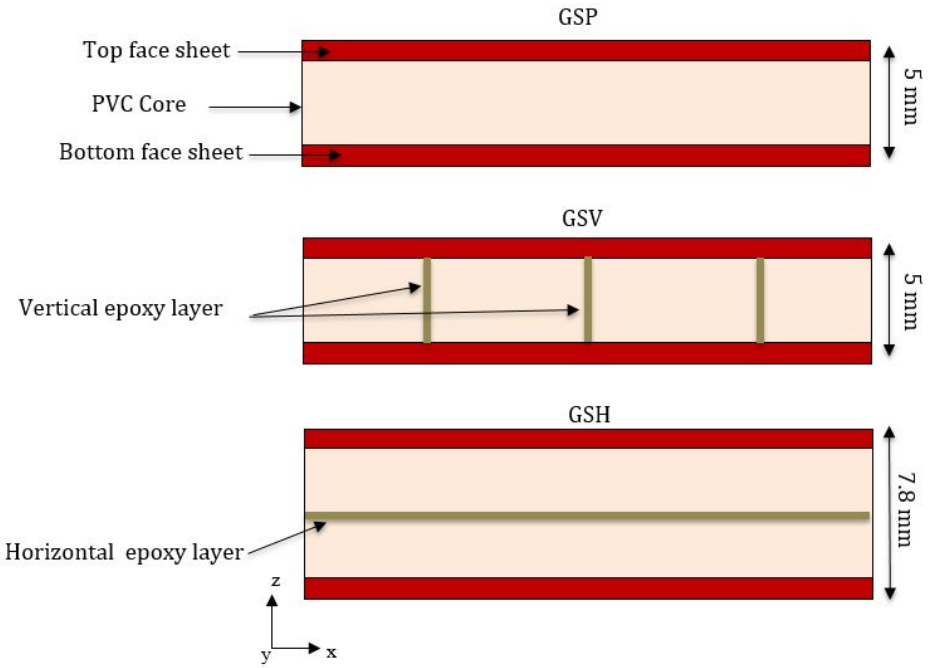

Fig. 1: Sample configuration.

Tab. 1: Mechanical properties of FRPSS constituents (Osa-Uwagboe et al., 2023b)

Materials	Young's Modulus (GPa)	Shear Modulus (GPa)	Poisson's Ratio	Density (g/cm^3)
GFRP face sheets	12.96	7.65	0.16	2.25
PVC core	0.075	0.027	-	0.075
Epoxy	1.72	-	0.29	1.16

Tab. 2: Sample nomenclature

Nomenclature	Description
GSPu	GFRP sandwich without epoxy layer before exposure
GSPe	GFRP sandwich without epoxy layer after exposure
GSVu	GFRP sandwich with vertical epoxy layer before exposure
GSVe	GFRP sandwich with vertical epoxy layer after exposure
GSHu	GFRP sandwich with horizontal epoxy layer before exposure
GSHe	GFRP sandwich with horizontal epoxy layer after exposure

2.2 Seawater exposure

According to ASTM B117-19 ASTM, International (2019a) samples were placed in an Ascott S450 salt-spray chamber (Ascott Analytical Equipment Ltd, UK) with seawater salinity of 3.3 per cent and a temperature of 40°C. This temperature, below the glass transition point, prevents temperature-induced damage. The pH level was kept constant to avoid chemical reactions between the samples, focusing on the effects of seawater exposure on mechanical behavior. Periodic gravimetric measurements determined moisture gain in exposed samples. During the exposure, salt-water penetrated the samples, with average moisture uptake M increasing over time, defined as

$$M = \left(\frac{M_t - M_o}{M_o}\right) \times 100\% \tag{1}$$

where M is the moisture increase (in percent) while M_t and M_o are the mass of the samples before and after seawater exposure, respectively.

2.3 Moisture monitoring with acoustic emission

Acoustic-emission (AE) signals were captured using a Micro-SHM system (Physical Acoustics Corporation, USA) operating in the range between 1 kHz and 1 MHz, with 4 AE channels and 2 parametric channels. In this study, two channels were linked to

Nano-30 AE sensors (125 kHz–750 kHz). The AE wave velocity in FRPSS is influenced by the elastic modulus of the face sheets, constituent density, and the thickness of the core and skin. A pencil break (Hsu-Nielsen) test was used to monitor the moisture ingress in Type A (GSP) samples without adhesive layers and Type B (GSV/GSH) samples with such layers, assessing the impact of core thickness and configuration. AE accuracy was validated with conventional weighing methods, providing a non-invasive, practical strategy for in situ degradation monitoring of marine vessels, bypassing costly and time-consuming experimental methods. The AE wave velocity is calculated as follows:

$$v = \left(\frac{D}{t_2 - t_1} \right) \tag{2}$$

where D is the separation distance between sensors 1 and 2 while t_1 and t_2 are the times of maximum amplitude at sensors 1 and 2 respectively.

2.4 Low-velocity impact test

A large-deflection dynamic bending test was conducted using an unnotched cantilever setup per ASTM D4812 ASTM, International (2019b). An instrumented pendulum-type RESIL impactor with a 1.5 mm radius, 0.23 m arm length, and 0.46 kg mass was used, with data processed by a DAS 8000 acquisition system. Rectangular specimens (80 mm x 15 mm) were clamped 27 mm from the base, with the impact zone 22 mm above the clamp. Single-impact tests were conducted on specimens before and after seawater exposure to assess the effects of moisture uptake on the FRPSS. A hammer release angle of 150° with an impact speed of 2.9 m/s, corresponding to 1.93 J of energy, was used to avoid visible damage. Several iterations ensured the correct striker angle and number of impacts to achieve noticeable damage across all samples. A total of 5 samples per configuration was used for the experiments and the average values presented to ensure repeatability. The experimental setup for the impact bending test is presented in Fig. 2.

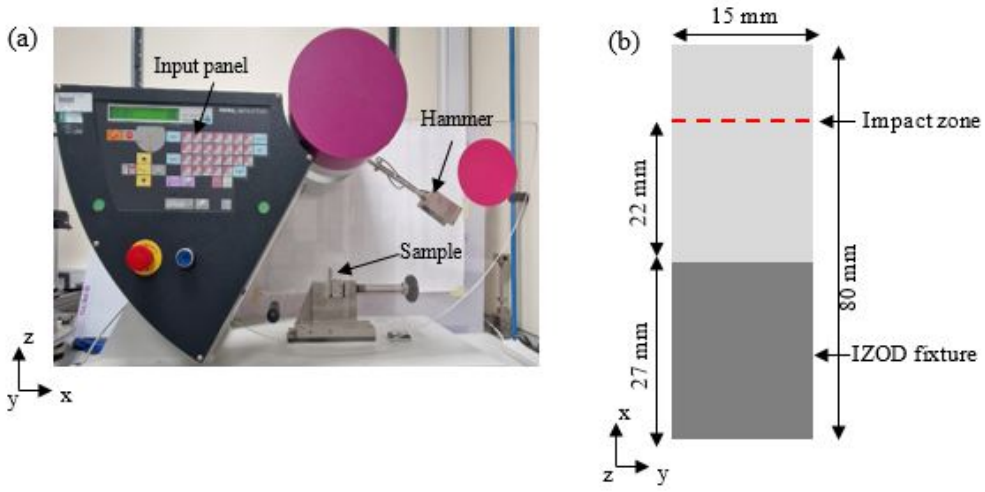

Fig. 2: Out-of-plane impact bending experimental set-up.

2.5 Post-mortem analysis

This study focused on examining the macro/meso-scale post-mortem damage of specimens after impact. Given that impact energy was absorbed by internal damage mechanisms, assessing this damage reveals the impact of moisture uptake on the samples. To accomplish this, a high-resolution NIKON XTH X-Tex 160Xi X-ray micro-CT system (NIKON Metrology Europe, Leuven, Belgium) was employed. The X-ray system used a pixel size of 27.79 μm, with an exposure time of 1 s and settings of 65 kV, 68 μA, and 4.2 W for energy, current, and power, respectively. Post-processing was carried out using VG Studio Max 3.1 and Dragonfly ORS software for image reconstruction and damage analysis.

3 Results

3.1 Assessment of moisture uptake

The obtained moisture absorption curves adhere to Fickian diffusion, with a sharp increase during the initial exposure. The pure sandwich specimen absorbed more moisture (5.5%) than the GSV (2.4%) and GSH (3.4%) samples. This was because the pure sandwich had less resistance to diffusion once the matrix plasticizes, unlike GSV and GSH, which need more epoxy plasticization. GSH samples showed lower moisture absorption, indicating that moisture mainly penetrated in the in-plane direction with minimal edge effects. All the studied samples eventually reached saturation, as shown by the plateau in the curves. GSP took longer to reach saturation compared to GSV and GSH, suggesting that adhesive cores led to moisture-absorption properties similar to the epoxy layers. The moisture uptake is shown in Fig. 3. It is worth noting that although the chart shows a predefined profile, there

are several kinks in the moisture uptake which could be attributed to the dissimilarity of the heterogeneous FRPSS specimen thereby affecting their interaction with water molecules as well as the presence of impurities during the manufacturing process.

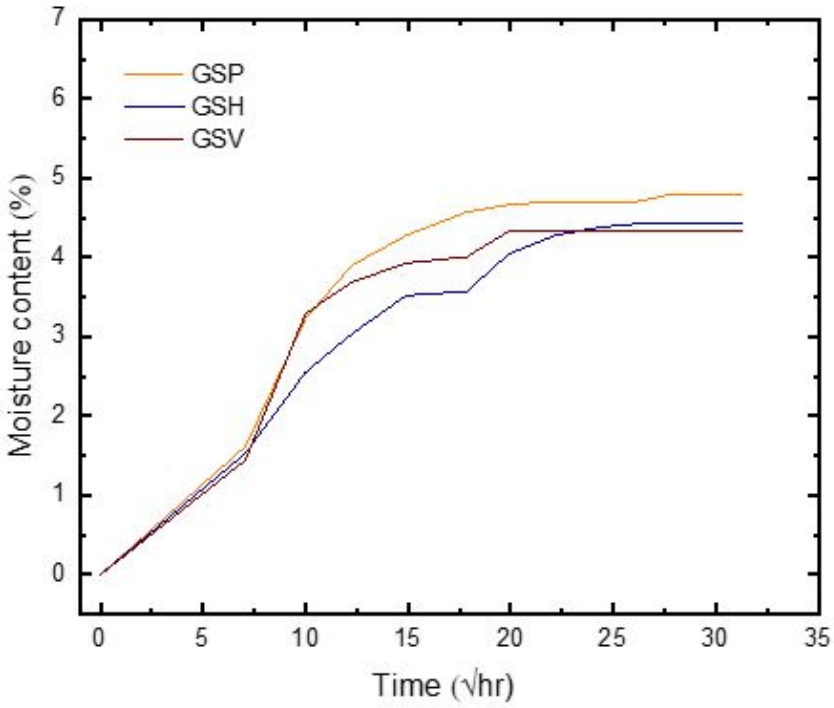

Fig. 3: Evolution of moisture content with time in FRPSSs.

3.2 Moisture monitoring with AE

To relate the AE feature to moisture absorption, the average velocity is analysed with respect to the moisture content of the two specimens. The data showed that the AE velocity decreased until reaching saturation, falling from 1788.6 m/s to 1335.5 m/s (a 31% decrease) for Type A, and from 2496.6 m/s to 1485.2 m/s (a 48% decrease) for Type B. The more significant reduction observed in Type B can be linked to the degradation of the adhesive layers. This proves that the AE features could capture the polymerization caused by seawater exposure (indicated by a higher degradation of the matrix/fiber interface as well as the reduction in adhesion between the facesheets and the core). Thereby establishing this use of AE as a viable tool for scheduled maintenance of FRPSS for marine use.

3.3 Impact load-time assessment

In a single-impact test, the load-time impact behavior of FRPSS before and after seawater exposure is presented in Fig. 4. The global peak load, known as the Hertzian failure point, marks the onset of damage, primarily matrix cracking, with potential for through-thickness delamination and core/face sheet disbonding. It can be seen that at a constant energy level of 1.93 J, the peak loads which depicts the damage resistance of the specimen could be used to determine the effects of moisture uptake on the samples past seawater exposure. From Fig. 4, there is a sharp decline in the load for all sample types, indicative of severe damage modes including delamination, facesheet/core debonding, and fiber fracture.It should be noted that the GSP specimen experienced the most significant decrease in force, with a 39.1% reduction, while the GSV and GSH specimens saw reductions of 7.2% and 15.9%, respectively. This greater reduction in GSP could be linked to the absence of adhesive epoxy layers in its core thereby liminting its damage resistance after exposure.

3.4 Energy-time results

Fig. 5 illustrates the energy absorption characteristics of FRPSS specimens subjected to a single impact, both before and after seawater exposure. The data showed that the GSP and GSH specimens absorbed 95% of the impact energy, while the GSV specimen had an absorption rate of 89%. There was minimal difference in absorbed energy between the exposed and unexposed samples. This observation may suggest an increase in damping effects or a transition in failure mode from brittle fracture to a more ductile mode, possibly due to plasticization and swelling of the matrix with an increased moisture uptake. Another possible explanation for this phenomenon could be a more uniform redistribution of stresses due to moisture absorption, leading to a reduction in impact forces while maintaining similar energy absorption after seawater exposure. Similar behaviour of composite materials following the environmental exposure was documented in Chawla (2019).

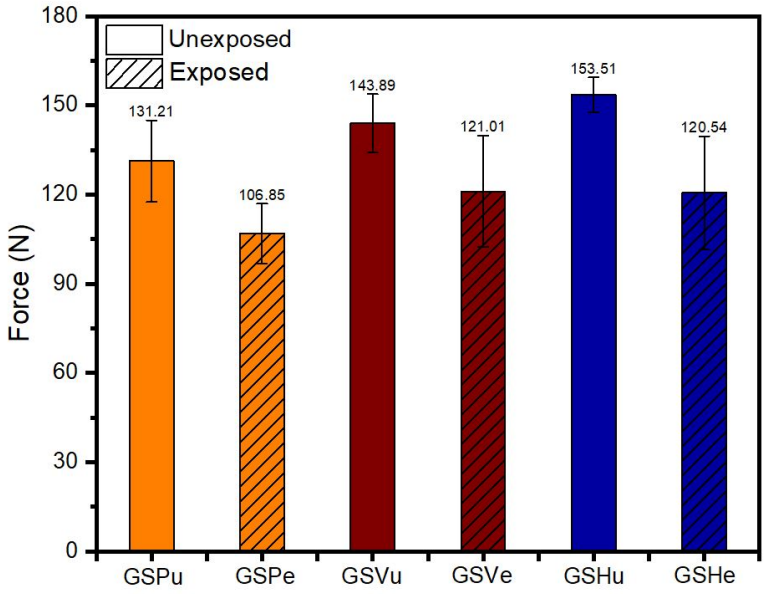

Fig. 4: Impact force - time curve of FRPSS samples.

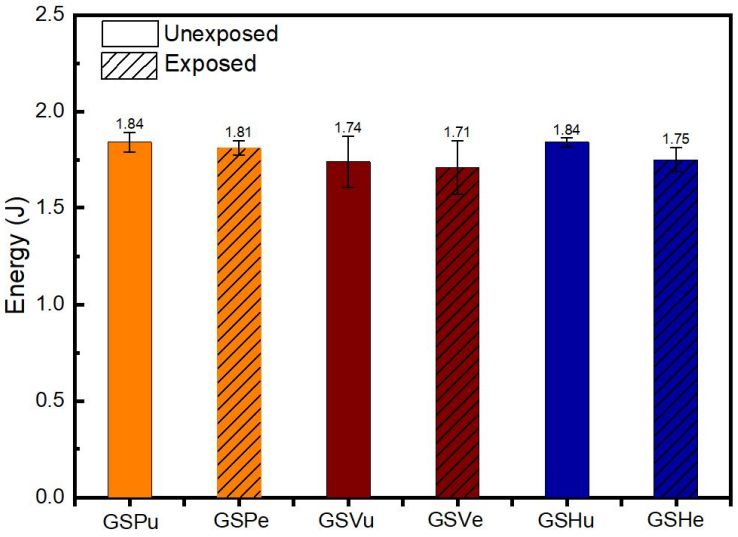

Fig. 5: Energy - time curve of FRPSS samples.

3.5 Post-mortem analysis

Fig. 6 show x-ray micro-CT images of FRPSS samples (both exposed and unexposed) after bending impacts. The images reveal a range of damage modes, including matrix cracking, core shearing, delamination, core/facesheet debonding, and fiber breakage, with varying levels of severity across all samples. Generally, the most severe damage, characterized by facesheet rupture, was found in the clamped region due to the high stress concentration from the applied boundary conditions. Consequently, extensive damage was observed on the back of the specimen.

4 Conclusion

This paper examined the impact bending properties of FRPSS after seawater exposure with moisture intake monitored using an AE approach, and assessing internal damage morphology. The study demonstrated that the moisture uptake of GSP, GSV, and GSH samples followed a Fickian diffusion curve, reaching saturation at 5.5%, 2.4%, and 3.4%, respectively, after 978 hours. The lower moisture uptake in GSV and GSH samples could be attributed to the obstruction to the diffusion process once matrix plasticization began in type B samples. GSP took longer to reach saturation compared to GSV and GSH, which saturated almost simultaneously Also, all specimens showed reduced damage-resistance properties after seawater exposure under impact. GSP experienced the largest reduction in force at 39.1% after seawater exposure, while GSV and GSH showed reductions of 7.2% and 15.9%, respectively. This could be due to the additional stiffness offered by the adhesive layers in the core coupled with the limited effects of seawater ageing in the through-thickness direction. However, there was minimal change in absorbed energy between exposed and unexposed specimens. Main damage modes experienced as a result of seawater ageing were intensified core shearing,

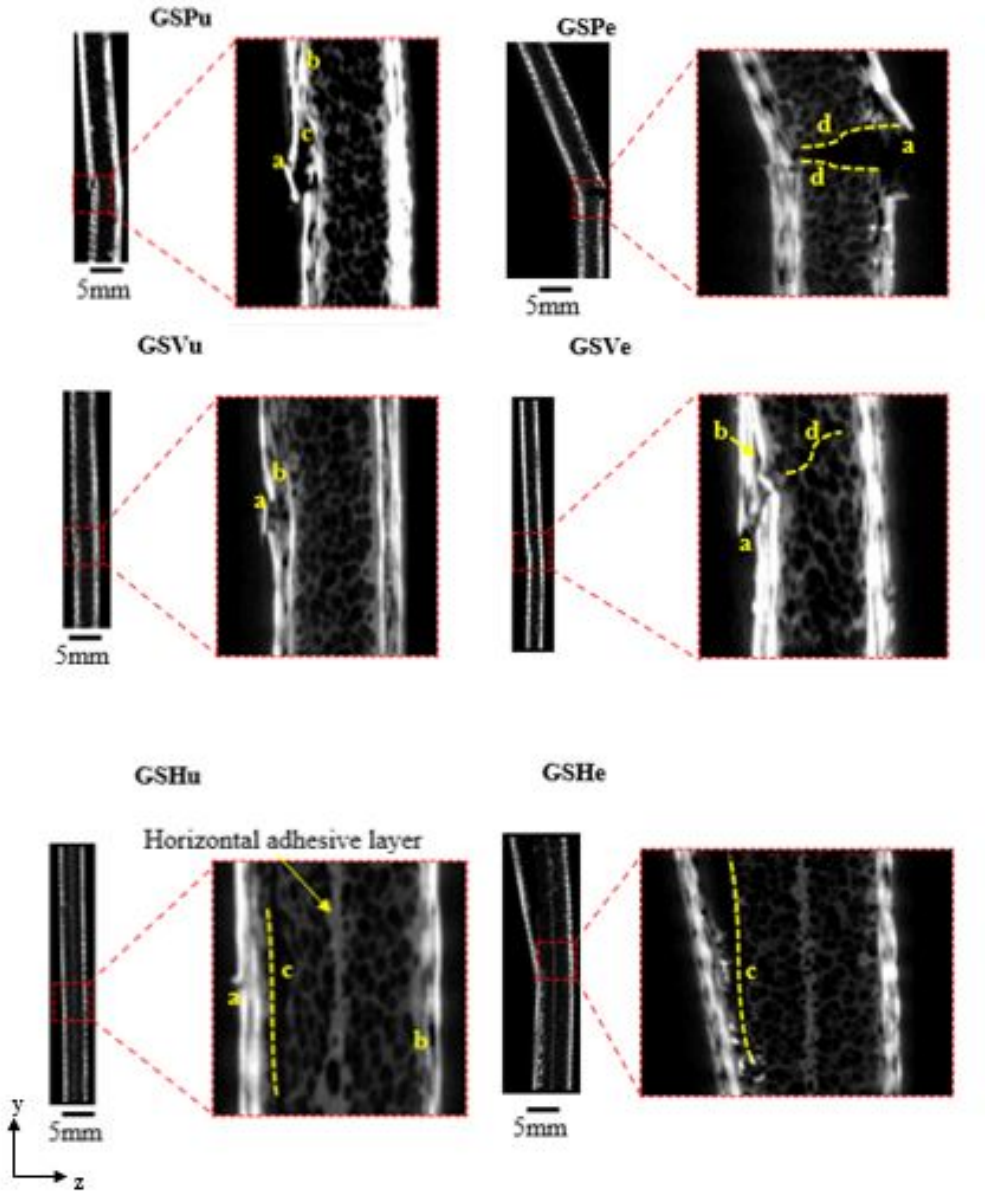

Fig. 6: X-ray micro-CT analysis of FRPSS samples. Note: a – fibre breakage, b – delamination, c - face sheet/core debonding and d – core shearing.

delamination, fibre breakage and facesheet/core debonding.

References

ASTM, International. *Standard Practice for Modified Salt Spray (Fog) Testing 1*. Annual Book of ASTM Standards. 2019a. URL https://doi.org/10.1520/G0085-19.

ASTM, International. *Standard Test Method for Unnotched Cantilever Beam Impact Resistance of Plastics 1*. Annual Book of ASTM Standards. 2019b. URL https://doi.org/10.1520/D4812-19E01.

GB Chai and S Zhu. A review of low-velocity impact on sandwich structures. *Proceedings of the Institution of Mechanical Engineers, Part L: Journal of Materials: Design and Applications*, 225:207–230, 2011. doi: 10.1177/1464420711409985.

KK Chawla. *Composite Materials*. Springer International Publishing, Cham, 2019. doi: 10.1007/978-3-030-28983-6.

D Feng and F Aymerich. Damage prediction in composite sandwich panels subjected to low-velocity impact. *Composites Part A: Applied Science and Manufacturing*, 52:12–22, 2013. doi: 10.1016/j.compositesa.2013.04.010.

N Osa-Uwagboe, VV Silberschimdt, A Aremi, and E Demirci. Mechanical behaviour of fabric-reinforced plastic sandwich structures: A state-of-the-art review. *Journal of Sandwich Structures & Materials*, 2023a. doi: 10.1177/10996362231170405.

N Osa-Uwagboe, AG Udu, VV Silberschmidt, KP Baxevanakis, and E Demirci. Damage assessment of glass-fibre-reinforced plastic structures under quasi-static indentation with acoustic emission. *Materials*, 16:5036, 2023b. doi: 10.3390/ma16145036.

N Osa-Uwagboe, VV Silberschimdt, and E Demirci. Seawater effect on energy-absorption properties of polymer-based composite sandwich structures. *Procedia Structural Integrity*, 54:44–51, 2024. doi: 10.1016/j.prostr.2024.01.054.

Y Qiu, R Yan, W Shen, X Li, and Z Ye. Load-bearing characteristics of marine complex sandwich composites considering unequal elastic modulus in tension and compression. *Marine Structures*, 89:103382, 2023. doi: 10.1016/j.marstruc.2023.103382.

A Robin, P Davies, M Arhant, S Le Jeune, N Lacotte, E Morineau, et al. Mechanical performance of sandwich materials with reduced environmental impact for marine structures. *Journal of Sandwich Structures & Materials*, 2023. doi: 10.1177/10996362221127975.